Sampling microcanonical measures of the 2D Euler equations through Creutz's algorithm: a

phase transition from disorder to order when energy is increased

Sampling microcanonical measures of the 2D Euler equations through Creutz's algorithm: a phase transition from disorder to order when energy is increased

Max Potters[1,2], Timothee Vaillant[2] and Freddy Bouchet[2]

[1] Laboratoire de Physique de l'École Normale Supérieure de Lyon, Université de Lyon, CNRS, 46 Allée d'Italie, 69364 Lyon cédex 07, France
[2] Delft Center for Systems and Control, Delft University of Technology, Mekelweg 2, 2628 CD Delft, The Netherlands
E-mail: m.g.potters@tudelft.nl, timothy.vaillant@ens-lyon.fr and Freddy.Bouchet@ens-lyon.fr

Abstract. The 2D Euler equations are basic examples of fluid models for which a microcanonical measure can be constructed from first principles. This measure is defined through finite-dimensional approximations and a limiting procedure. Creutz's algorithm is a microcanonical generalization of the Metropolis–Hastings algorithm (to sample Gibbs measures, in the canonical ensemble). We prove that Creutz's algorithm can sample finite-dimensional approximations of the 2D Euler microcanonical measures (incorporating fixed energy and other invariants). This is essential as microcanonical and canonical measures are known to be inequivalent at some values of energy and vorticity distribution. Creutz's algorithm is used to check predictions from the mean-field statistical mechanics theory of the 2D Euler equations (the Robert–Sommeria–Miller theory). We find full agreement with theory. Three different ways to compute the temperature give consistent results. Using Creutz's algorithm, a first-order phase transition never observed previously and a situation of statistical ensemble inequivalence are found and studied. Strikingly, and in contrast to the usual statistical mechanics interpretations, this phase transition appears from a disordered phase to an

ordered phase (with fewer symmetries) when the energy is increased. We explain this paradox.

Contents

1. Introduction

Two-dimensional and geophysical flows are highly turbulent, yet embody large-scale coherent structures such as ocean rings, jets, and large-scale vortices. Understanding how these structures appear and predicting their shape is a major theoretical challenge. The statistical mechanics approach to geophysical flows is a powerful complement to more conventional theoretical and numerical methods (see [1] for a recent review, or [2]–[4] for related approaches). In the inertial limit statistical equilibria describe, with only a few thermodynamical parameters, the main natural attractors of the dynamics.

Recent studies in quasi-geostrophic models provide encouraging results: a model of the Great Red Spot of Jupiter [5], and explanations of several different phenomena: the drift properties of ocean rings [6], the inertial structure of mid-basin eastward jets [6], bistability in complex turbulent flows [7], and so on.

Generalization to more comprehensive hydrodynamical models, which can simulate gravity-wave dynamics and enable energy transfer through wave motion, would be interesting. Both of the aforementioned processes are essential in understanding the geophysical flow energy balance. However, due to difficulties in essential theoretical parts of the statistical mechanics approach, previous methods describing statistical equilibria have been up to now limited to the use of quasi-geostrophic, or simpler, models. In order to study the statistical mechanics of these models, it would be useful to be able to rely on numerical sampling of their microcanonical measures.

The 2D Euler equations can be formulated in terms of the vorticity field. Points in the vorticity field are coupled through a long-range interaction. In contrast with traditional systems, long-range interaction systems are well known to show generic inequivalence between microcanonical and canonical ensembles ([8]–[12], see [8] for a classification). The microcanonical ensemble is richer than the canonical one, as the canonical equilibrium states form a subset of the microcanonical equilibrium states [12, 13]. For these systems it is thus essential to be able to sample microcanonical measures instead of canonical ones.

Creutz's algorithm [14] is a Monte Carlo approach used to sample microcanonical measures of discrete spin systems [15, 16]. Whereas the Metropolis–Hastings algorithm samples Gibbs measures (canonical ensemble), the Creutz algorithm imposes an energy constraint and thus samples the microcanonical measure (microcanonical ensemble). Section 3 gives a proof of detailed balance and convergence to the microcanonical measure for Creutz's algorithm. Appendix A defines the classical concepts useful for the discussion of detailed balance. Appendix B also describes some improper interpretation of the algorithm that may lead to wrong results.

The main aim of this paper is to discuss the first generalization of Creutz's algorithm to hydrodynamical systems. The main novelty is the ability to deal with the statistical mechanics of fields rather than discrete variables. For this first work, we consider the 2D Euler equations and precisely define the microcanonical measures through finite-dimensional approximations and a limiting procedure. The generalization to the quasi-geostrophic model or the Vlasov equation, the microcanonical measure definition and their sampling through Creutz's algorithm would be straightforward. The method is extremely robust and could also be easily generalized to more complex models like the 3D axisymmetric Euler equations or the shallow water model.

The 2D Euler equations and related models have an infinite number of conserved quantities, called Casimirs. Michel and Robert [17] first discussed the use of large-deviation theory as a justification of mean-field variational problems for the microcanonical measure. Later on, Ellis and collaborators [18] defined approximations of equilibrium measures, through a description of the fields over a lattice, where N^2 is the number of degrees of freedom (lattice site). In this work, Ellis and Turkington treated the energy constraint microcanonically and the Casimir constraints canonically. They proved that these approximate measures verify a large-deviation principle, where N^2 is the large-deviation rate. In this paper, we study an N^2-degrees-of-freedom discretized approximation of equilibrium measures (following Ellis and collaborators), but treating all constraints microcanonically (as did Robert and Michel). This slightly different presentation is an improvement, as proceeding through discretization provides a clear and straightforward definition of the microcanonical measures, and the set of microcanonical equilibrium states includes the set of canonical equilibrium states (see the beginning of section 1). The limit is then an invariant measure of the 2D Euler equations [19].

As was already clear in previous works [17, 18] (please see the detailed discussion in [1]), the 2D Euler equations show mean-field behavior. It is therefore natural to define macrostates through coarse graining of microstates. The most probable macrostate maximizes an entropy functional with energy constraints. The mean-field entropy for the macrostate is justified as being the opposite of a large-deviation rate function, where N^2 is the large-deviation rate. We explain these theoretical results and their justification at a heuristic level in this paper.

These theoretical results (the concentration of most microstates on a single predicted macrostate maximizing a mean-field variational problem) provide a very interesting case for testing Creutz's algorithm with numerical results. This test possibility was our main motivation for devising this algorithm for the 2D Euler equations, before generalizing to more complex models for which mean-field type large-deviation results are not yet available.

We have checked that the numerical results are in full agreement with the theoretical predictions from the mean-field variational problem. Independently of the mean-field variational problem, Creutz's algorithm provides a very simple and robust way to sample microcanonical measures. For instance, we have used it to describe previously unknown first-order phase transitions between dipole and parallel flows in a doubly periodic domain.

Previous works considered Monte Carlo simulations for the 2D Euler equations or related models (see, for instance, a very interesting application to oceans in [20] and references therein, or [2]). However, these works always sampled the canonical energy–enstrophy measures (using the Metropolis–Hastings algorithm and not considering other invariants). These methods thus provide only a very small subset of the equilibrium measures of these models.

Dubinkina and Frank [21] recently proposed a very nice particle-mesh algorithm for the 2D Euler equations that conserves the vorticity distribution. This algorithm is also a way to sample microcanonical measures, as was shown in their paper. As a positive point, the dynamics of the particle-mesh method is a good approximation of the 2D Euler dynamics for finite times (whereas the Creutz algorithm is just a sampling of the microcanonical measure). One drawback of the particle-mesh algorithm is that ergodicity has to be assumed. Moreover, it seems that this particle-mesh approach with potential

4

vorticity conservation has so far not been proven to be generalizable to more complex models (for instance the shallow water model).

We also note that other numerical algorithms exist to compute equilibrium states for the 2D Euler equations: the Turkington and Whitaker algorithm [22, 23], relaxation equations [24], or continuation algorithms [7, 25] (please see [1] for a description of these algorithms). However, these three algorithms compute extrema or critical points of the mean-field variational problem. They thus rely on large-deviation theoretical results that are so far not known to exist for more complex models, like for instance the 3D axisymmetric equations or the shallow water models.

In this paper we also discuss the discovery of a first-order phase transition in the microcanonical ensemble, found using Creutz's algorithm for the 2D Euler equations. This phase transition is striking in many respects. It is a first-order phase transition in the microcanonical ensemble, which is a thermodynamical curiosity (see [8]). As discussed in detail in [8], such a first-order phase transition in the microcanonical ensemble is a sign of ensemble inequivalence, as the entropy curve cannot be concave at such a transition point. Moreover, it is a transition from a disordered state towards an ordered state when the energy is increased, in contrast with what could be expected from classical statistical mechanics arguments. This paradox is due to the negative temperature of the system. Indeed, then the entropy, the measure of disorder, decreases when the energy increases. We discuss this point further in section 5. From a fluid mechanics point of view, this transition is a drastic change of the flow topology from a dipole to a parallel flow. A very interesting recent example of two different phase transitions in two different statistical ensembles is discussed in [26].

The outline of this paper is as follows. In section 2, the 2D Euler equations are introduced. The statistical mechanics theory is treated, as well as the finite-dimensional approximation of the 2D Euler microcanonical measure. Section 3 provides a proof of why Creutz's algorithm samples microcanonical measures. Theoretical predictions from the microcanonical mean-field variational problem presented in section 2 are confronted with numerical results in section 4, where we focus mainly on the negative temperature of the system. In section 5, examples of phase transitions and an example of ensemble inequivalence are discussed. In this section, we also discuss the transition from a disordered state to an ordered one upon increasing energy. Section 6 provides some perspectives and we give comments for future work.

2. Statistical mechanics of the 2D Euler equations

2.1. The 2D Euler equations and invariants

The 2D Euler equations are given by

$$\partial_t \omega + \mathbf{v} \cdot \boldsymbol{\nabla} \omega = 0, \qquad \mathbf{v} = \mathbf{e}_z \times \boldsymbol{\nabla} \psi, \qquad \text{and} \qquad \omega = \Delta \psi, \tag{1}$$

where $\omega = (\boldsymbol{\nabla} \times \mathbf{v}) \cdot \mathbf{e}_z$ is the vorticity, and $\mathbf{v}$ is the non-divergent velocity expressed as the curl of the stream function ψ. The stream function is defined up to a constant, which is set to zero without loss of generality. The relation $\omega = \Delta \psi$ is complemented with doubly periodic boundary conditions on a domain given by $\mathscr{D} = [0, 1) \times [0, 1)$ and $\mathbf{r} = (x, y)$. The

energy of the flow reads

$$\mathscr{E}[\omega] = \tfrac{1}{2} \int_{\mathscr{D}} \mathrm{d}^2\mathbf{r}\,\mathbf{v}^2 = \tfrac{1}{2} \int_{\mathscr{D}} \mathrm{d}^2\mathbf{r}\,(\nabla\psi)^2 = -\tfrac{1}{2} \int_{\mathscr{D}} \mathrm{d}^2\mathbf{r}\,\omega\psi. \tag{2}$$

The energy is conserved, i.e. $d_t\mathscr{E} = 0$. The equations also conserve an infinite number of functionals, named Casimirs. These are related to the degenerate structure of the infinite-dimensional Hamiltonian system and can be understood as invariants arising from Noether's theorem [27]. These functionals are of the form

$$\mathscr{C}_s[\omega] = \int_{\mathscr{D}} \mathrm{d}^2\mathbf{r}\,s(\omega), \tag{3}$$

where s is any sufficiently smooth function depending on the vorticity field. We note that on a doubly periodic domain the total circulation is zero,

$$\Gamma = \int_{\mathscr{D}} \mathrm{d}^2\mathbf{r}\,\omega = 0. \tag{4}$$

A special Casimir is

$$C(\sigma) = \int_{\mathcal{D}} \mathrm{d}^2\mathbf{r}\,H(-\omega + \sigma), \tag{5}$$

where $H(\cdot)$ is the Heaviside step function. This Casimir returns the area of $B(\sigma) = \{\mathbf{r} \mid \omega(\mathbf{r}) \leq \sigma\}$, i.e. the domain of all vorticity levels smaller than or equal to σ. $C(\sigma)$ is an invariant for any σ and therefore any derivative of it as well. Therefore, the distribution of vorticity, defined as $D(\sigma) = C'(\sigma)$, where the prime denotes a derivation with respect to σ, is also conserved by the dynamics. The expression $D(\sigma)\,\mathrm{d}\sigma$ is the area occupied by the vorticity levels in the range $\sigma \leq \omega \leq \sigma + \mathrm{d}\sigma$.

Moreover, any Casimir can be written in the form

$$\mathcal{C}_{\mathrm{f}}[\omega] = \int \mathrm{d}\sigma\,f(\sigma)\,D(\sigma). \tag{6}$$

The conservation of all Casimirs (equation (3)) is therefore equivalent to the conservation of $D(\sigma)$.

The conservation of the distribution of vorticity levels can also be understood from the equations of motion, cf equation (1). We find that $D\omega/\mathrm{d}t = 0$, showing that the values of the vorticity field are Lagrangian tracers. This means that the values of ω are transported through the non-divergent velocity field, thus keeping the distribution unchanged. The Casimirs and energy are the invariants of the 2D Euler equations. Their existence plays a crucial role in the dynamics of the system.

From now on, we restrict ourselves to a K-level vorticity distribution. We make this choice for pedagogical reasons, but the generalization to a continuous vorticity distribution is straightforward. The K-level vorticity distribution is defined as

$$D(\sigma) = \sum_{k=1}^{K} A_k \delta(\sigma - \sigma_k), \tag{7}$$

where A_k denotes the area occupied by the vorticity value σ_k. The areas A_k are not arbitrary as their sum must obey $\sum_{k=1}^{K} A_k = |\mathscr{D}| = 1$ (the total area of the domain is

equal to unity). Moreover, the boundary condition (equation (4)) imposes the constraint $\sum_{k=1}^{K} A_k \sigma_k = 0$.

2.2. Microcanonical measure

As the 2D Euler equation is a conservation law (the time derivative of ω is the divergence of a current), it verifies a formal Liouville theorem [28, 29]. This formally justifies that the microcanonical measure will be dynamically invariant. In order to properly identify a microcanonical measure, we will thus discretize the vorticity field in finite-dimensional space, with N^2 degrees of freedom, and then take the limit $N \to \infty$. As any point in the physical space has a symmetric role, a uniform grid has to be chosen in order to preserve the volume conservation corresponding to the Liouville theorem.

We denote the lattice points by $\mathbf{r}_{ij} = (i/N, j/N)$, with $0 \leq i, j \leq N - 1$, and denote $\omega_{ij}^N = \omega(\mathbf{r}_{ij})$ to be the vorticity value at point $\mathbf{r}_{ij}$. The total number of points is N^2.

As discussed in section 2.1, we assume $D(\sigma) = \sum_{k=1}^{K} A_k \delta(\sigma - \sigma_k)$. For this finite-$N$ approximation, our set of microstates (configuration space) is then

$$X_N = \left\{ \omega^N = (\omega_{ij}^N)_{0 \leq i,j \leq N-1} \mid \forall i, j \ \omega_{ij}^N \in \{\sigma_1, \ldots, \sigma_K\}, \quad \text{and} \right.$$
$$\left. \forall k \ \# \left\{ \omega_{ij}^N \mid \omega_{ij}^N = \sigma_k \right\} = N^2 A_k \right\}. \tag{8}$$

Here, $\#(A)$ is the cardinality of set A. We note that X_N depends on $D(\sigma)$ through A_k and σ_k (see equation (7)). We note that all microstates in X_N have the proper vorticity distribution.

In order to define a microcanonical ensemble, we also have to impose an energy constraint. Using the above expression we define the energy shell $\Gamma_N(E, \Delta E)$ as

$$\Gamma_N(E, \Delta E) = \left\{ \omega^N \in \Gamma_N \mid E_0 \leq \mathscr{E}_N[\omega^N] \leq E_0 + \Delta E \right\}, \tag{9}$$

where

$$\mathscr{E}_N = \frac{1}{2N^2} \sum_{i,j=0}^{N-1} \left(\mathbf{v}_{ij}^N \right)^2 = -\frac{1}{2N^2} \sum_{i,j,i',j'=0}^{N-1} \omega_{ij}^N G_{ij,i'j'} \omega_{i'j'}^N \tag{10}$$

is the finite-N approximation of the system energy, with $\mathbf{v}_{ij}^N = \mathbf{v}(\mathbf{r}_{ij})$ being the discretized velocity field, ΔE is the width of the energy shell, and $G_{ij,i'j'}$ is a finite-N approximation of the Laplacian Green function on domain $\mathscr{D}$. We shall define these finite-N approximate fields more precisely in section 3. Note that a finite width of the energy shell is necessary for our discrete approximation, as the cardinality of X_N is finite. Indeed, the set of accessible energies on X_N is also finite. Let $\Delta_N E$ be the typical difference between two successive achievable energies. We therefore assume that $\Delta_N E \ll \Delta E \ll E_0$.

The fundamental assumption of statistical mechanics states that all microstates in this ensemble are equiprobable. By virtue of this assumption, the probability to observe any microstate is $\Omega_N^{-1}(E_0, \Delta E)$, where $\Omega_N(E_0, \Delta E)$ is the number of accessible microstates and is defined as the cardinality of the set $\Gamma_N(E_0, \Delta E)$. The finite-N specific Boltzmann entropy is then given by

$$S_N(E_0, \Delta E) = \frac{1}{N^2} \log \Omega_N(E_0, \Delta E). \tag{11}$$

The microcanonical measure is defined through the expectation values of any observable $\mathscr{A}$. For any observable $\mathscr{A}[\omega]$ (for instance a smooth functional of the vorticity field), we refer to its finite-N approximation by $\mathscr{A}_N[\omega^N]$. The expectation value of $\mathscr{A}_N$ for the microcanonical measure reads

$$\langle \mu_N(E_0, \Delta E),\, \mathscr{A}_N(\omega^N) \rangle \equiv \langle \mathscr{A}_N(\omega^N) \rangle_N \equiv \frac{1}{\Omega_N(E_0, \Delta E)} \sum_{\omega^N \in \Gamma_N(E_0, \Delta E)} \mathscr{A}_N(\omega^N). \tag{12}$$

The microcanonical measure μ for the 2D Euler equation is defined as a limit of the finite-N measure,

$$\langle \mu(E_0),\, \mathscr{A}(\omega) \rangle \equiv \lim_{N \to \infty} \langle \mu_N(E_0, \Delta E),\, \mathscr{A}_N(\omega^N) \rangle. \tag{13}$$

The specific Boltzmann entropy is defined as

$$S(E_0) = \lim_{N \to \infty} S_N(E_0, \Delta E). \tag{14}$$

The limit measure and the entropy just defined are expected to be independent of ΔE in the limit $N \to \infty$. This will be justified in section 2.3 with large-deviation principles.

2.3. Sanov theorem and mean-field entropy

Computing the Boltzmann entropy by direct evaluation of equation (14) is usually an intractable problem. However, we shall give heuristic arguments in order to show that the limit $N \to \infty$ can be easily evaluated. The Boltzmann entropy (equation (14)) can then be computed through maximizing a constraint variational problem (called a mean-field variational problem, see equation (23)).

This variational problem is the foundation of the Robert–Sommeria–Miller (RSM) approach to the equilibrium statistical mechanics for the 2D Euler equations. The essential message is that the entropies computed from the mean-field variational problem (to be defined below) and from Boltzmann's entropy definition (equation (14)) are equal in the limit $N \to \infty$. The ability to compute the Boltzmann entropy through this type of variational problem is one of the cornerstones of statistical mechanics.

Our heuristic derivation is based on the same type of combinatoric argument as the ones used by Boltzmann for the interpretation of his H function in the theory of relaxation to equilibrium of a dilute gas. This derivation does not use the technicalities of large-deviation theory. The aim is to actually obtain the large-deviation interpretation of the entropy and to provide a heuristic understanding using basic mathematics only. The modern mathematical proof of the relation between the Boltzmann entropy and the mean-field variational problem involves the theory of large deviations and Sanov's theorem.

Macrostates are sets of microscopic configurations sharing similar macroscopic behavior. Our aim is to properly identify macrostates that fully describe the main features of the largest scales of 2D turbulent flows and compute their probability or entropy.

Let us first define macrostates through local coarse graining. We divide the $N \times N$ lattice into $(N/n) \times (N/n)$ non-overlapping boxes each containing n^2 grid points (n is an even number, and N is a multiple of n). These boxes are centered on sites $(i,j) = (In, Jn)$, where integers I and J verify $0 \leq I, J \leq N/n - 1$. The indices (I, J) label the boxes.

For any microstate $\omega^N \in \Gamma_N$, let $F_{k,IJ}^N$ be the frequency of finding a vorticity value σ_k in box (I, J),

$$F_{k,IJ}^N(\omega^N) = \frac{1}{n^2} \sum_{i=In-n/2+1}^{In+n/2} \sum_{j=Jn-n/2+1}^{Jn+n/2} \delta_d(\omega_{ij}^N - \sigma_k),$$

where $\delta_d(x)$ is equal to one whenever $x = 0$, and zero otherwise. We note that for all (I, J) $\sum_k F_{k,IJ}^N(\omega^N) = 1$.

A macrostate $p^N = \left\{ p_{k,IJ}^N \right\}_{0 \le I,J \le N/n-1; 1 \le k \le K}$, is the set of all microstates $\omega^N \in X_N$ such that $F_{k,IJ}^N(\omega^N) = p_{k,IJ}^N$ for all I, J, and k (by abuse of notation, and for simplicity, $p^N = \left\{ p_{k,IJ}^N \right\}_{0 \le I,J \le N/n-1; 1 \le k \le K}$ refers to both the set of values $p_{k,IJ}^N$ and the set of microstates having the corresponding frequencies). The property $\sum_k F_{k,IJ}^N(\omega^N) = 1$ imposes a local normalization constraint $\forall I, J \sum_k p_{k,IJ}^N = 1$. The entropy of the macrostate is defined as the logarithm of the number of microstates in the macrostate,

$$S_N[p^N] = \frac{1}{N^2} \log \# \left\{ \omega^N \in X_N | \text{ for all } I, J, \text{ and } k, \ F_{k,IJ}(\omega^N) = p_{k,IJ}^N \right\}. \tag{15}$$

From an argument by Boltzmann (a classical exercise in statistical mechanics), using combinatorics and the Stirling formula, and taking the limit $N > n \gg 1$, the asymptotical entropy of the macrostate is

$$S_N[p^N] \underset{N \gg n \gg 1}{\sim}$$

$$\begin{cases} \mathscr{S}_N[p^N] = -\dfrac{n^2}{N^2} \sum_{I,J=0}^{N/n-1} \sum_{k=1}^{K} p_{k,IJ}^N \log p_{k,IJ}^N & \text{if } \forall I, J \ \mathscr{N}[p_{IJ}] = 1 \quad \text{and} \quad \forall k \ \mathscr{A}_N[p_k^N] = A, \\ -\infty & \text{otherwise}, \end{cases}$$

where $\mathscr{N}[p_{IJ}^N] \equiv \sum_k p_{k,IJ}^N$. In large-deviation theory, this result could have been obtained using Sanov's theorem.

The coarse-grained vorticity is defined as

$$\overline{\omega_{IJ}^N} = \frac{1}{n^2} \sum_{i'=In-n/2+1}^{In+n/2} \sum_{j'=Jn-n/2+1}^{Jn+n/2} \omega_{i'j'}^N. \tag{16}$$

Note that, over the macrostate p^N, the coarse-grained vorticity depends on p^N only,

$$\overline{\omega_{IJ}^N} = \sum_{k=1}^{K} p_{k,IJ}^N \sigma_k \qquad \text{for } \omega^N \in p^N.$$

We now consider a new macrostate (p^N, E_0) which is the set of microstates ω^N with energy $\mathscr{E}_N[\omega^N]$ verifying $E_0 \le \mathscr{E}_N[\omega^N] \le E_0 + \Delta E$ (the intersection of $\Gamma_N(E, \Delta E)$ and p^N). For a given macrostate p^N, not all microstates have the same energy. Thus, the constraint on the microstate energy cannot be recast as a simple constraint on the macrostate p^N. Therefore, treating the energy constraint requires a more subtle approach. The energy (10) is

$$\mathscr{E}_N[\omega^N] = -\frac{1}{2N^4} \sum_{i,j,i',j'=0}^{N-1} \omega_{ij}^N G_{ij,i'j'} \omega_{i'j'}^N. \tag{17}$$

Then, in the limit $N \gg n \gg 1$, the variations of $G_{ij,i'j'}$ for (i', j') running over the small box (I, J) are vanishingly small. Hence, $G_{ij,i'j'}$ can be well approximated by the average value over the boxes $G_{IJ,I'J'}$,

$$G_{ij,i'j'} = G_{IJ,I'J'} + o\left(\frac{1}{n}\right). \tag{18}$$

From equation (17), using equations (16) and (18), it is easy to conclude that in the limit $N \gg n \gg 1$ the energy of any microstate of the macrostate p^N is very well approximated by the energy of the coarse-grained vorticity,

$$\mathscr{E}_N[\omega^N] \underset{N \gg n \gg 1}{\sim} \mathscr{E}_N[\overline{\omega_{IJ}^N}] = -\frac{n^2}{2N^2} \sum_{I,J=0}^{N/n-1} \overline{\omega_{IJ}^N} \psi_{IJ}^N,$$

where ψ_{IJ}^N is the stream function, and is related to the velocity field and vorticity field by equations (1). Note that in the above equation we made use of the relation $\mathscr{E}[\omega^N] = \mathscr{E}_N[\overline{\omega^N}] + o(1/n)$.

Hence, the Boltzmann entropy of the macrostate is

$$S_N[p^N, E_0] \underset{N \gg n \gg 1}{\sim} \begin{cases} \mathscr{S}_N[p^N] & \text{if } \forall k \; \mathscr{A}_N\left(p_k^N\right) = A_k, \quad \mathscr{N}[p^N] = 1 \quad \text{and} \quad \mathscr{E}_N[\overline{\omega_{IJ}^N}] = E_0, \\ -\infty & \text{otherwise.} \end{cases} \tag{19}$$

Consider $P_{N,E_0}(p^N)$ to be the probability density to observe the macrostate p^N. By definition of the microcanonical ensemble and of the entropies $S_N(E_0)$ (see equation (11)) and $S_N(p^N, E_0)$ (see equation (19)), we have

$$P_{N,E_0}(p^N) = \exp\left\{N^2\left[S_N[p^N, E_0] - S_N(E_0)\right]\right\}. \tag{20}$$

Let P_M be the probability density for the random variable X_M. The statement

$$\lim_{M \to \infty} -\frac{1}{M} \log\left[P_M(X_M = x)\right] = I(x) \tag{21}$$

is called a large-deviation result. $I(x)$ is the large-deviation rate function, and M the large-deviation rate. From this definition, we see that formula (20) is a large-deviation result for macrostate p^N for the macrocanonical measure. The large-deviation rate is N^2 and the large-deviation rate function is $-S_N[p^N, E_0] + S_N(E_0)$.

We now consider the continuous limit $n \to \infty$, $N \to \infty$. The macrostates p_k^N are now seen as finite-N approximations of p_k, the local probability to observe $\omega(\mathbf{r}) = \sigma_k$: $p_k(\mathbf{r}) = \langle\delta(\omega(\mathbf{r}) - \sigma_k)\rangle$. The macrostate is now characterized by $p = \{p_1, \ldots, p_K\}$. Taking the limit $N \gg n \gg 1$ allows us to define the entropy of the macrostate (p, E_0) as

$$S[p, E_0] =$$

$$\begin{cases} \mathscr{S}[p] \equiv -\sum_k \int_{\mathscr{D}} \mathrm{d}\mathbf{r} \, p_k \log p_k & \text{if } \forall k \; \mathscr{N}[p^k] = 1, \quad \mathscr{A}\left(p^k\right) = A_k \quad \text{and} \quad \mathscr{E}[\overline{\omega}] = E_0, \\ -\infty & \text{otherwise,} \end{cases} \tag{22}$$

where $\forall \mathbf{r}, \mathscr{N}(\mathbf{r}) = \sum_{k=1}^{K} p_k(\mathbf{r}) = 1$ is the local normalization. In the same limit, it is clearly seen from definition (15) and result (22) that there is a concentration of microstates close

to the most probable macrostate: the equilibrium state. The exponential concentration close to the equilibrium state is a large-deviation result, where the entropy appears as the opposite of a large-deviation rate function (up to a constant).

The exponential convergence towards this most probable state also justifies the approximation of the above entropy with the entropy of the most probable macrostate, equation (14), as

$$S(E_0) = \max_{\{p\}|\mathcal{N}(\mathbf{r})=1} \left\{ \mathscr{S}[p] \mid \mathscr{E}[\bar{\omega}] = E_0, \forall k \ \mathscr{A}(p^k) = A_k \right\}, \tag{23}$$

where $p = \{p_1, \ldots, p_K\}$, $\forall \mathbf{r} \ \mathcal{N}(\mathbf{r}) = \sum_{k=1}^{K} p_k(\mathbf{r}) = 1$ is the local normalization, $\mathscr{S}[p]$ is as defined in equation (22), and $\mathscr{A}[p_k]$ is the area of the domain corresponding to the vorticity value $\omega = \sigma_k$. The fact that the Boltzmann entropy $S(E_0)$ (equation (14)) can be computed from the variational problem (23) is a powerful non-trivial result from large-deviation theory.

In section 3, we shall test the prediction of concentration of microstates close to the equilibrium macrostate with numerical simulations. We first define Creutz's algorithm and explain why it is able to sample microcanonical measures. We continue by applying this algorithm to the 2D Euler equations.

3. Creutz's algorithm

Creutz's algorithm was introduced by Creutz in 1983 [14]. It is a generalization of the Metropolis–Hastings algorithm that samples the Gibbs measure (with a Boltzmann factor). Creutz's algorithm, on the other hand, samples the microcanonical measure in the energy shell $E_0 \leq \mathscr{E} \leq E_0 + \Delta E$ (a uniform distribution over the set $\Gamma_N(E_0, \Delta E)$). Here, the system energy is denoted by $\mathscr{E}$.

In section 3.1 we present Creutz's algorithm and prove that it actually samples the microcanonical measure. In section 3.2 we provide a method to calculate the inverse temperature β using this algorithm. We shall refer to appendix A for a precise definition of Markov chains, the detailed balance condition, and invariant measures (stationary distributions).

Creutz and others using his algorithm used the notion of a daemon. The aim of the daemon is to allow for slight energy fluctuations, which are necessary for systems with a discrete configuration space. With our notation the daemon energy E_d is nothing else than $E_\mathrm{d} = E_0 + \Delta E - \mathcal{E}$. The original Creutz algorithm samples a uniform measure over all microstates of energy smaller than $E_0 + \Delta E$. For this measure, in systems with positive temperature and a large number of degrees of freedom, the energy distribution is concentrated close to $E_0 + \Delta E$, and typical energy fluctuations are small.

In the 2D Euler case considered in this paper the temperature can be negative, as will be discussed in section 4.1.2. Microstates with the smallest possible energy then become overwhelmingly probable. In order to sample the microcanonical measure, we then need to impose a lower bound on the energy. In order to cope with all possible temperature cases we sample a uniform measure over the energy shell $E_0 \leq \mathscr{E} \leq E_0 + \Delta E$. Because of energy concentration properties, the microcanonical measure is independent of these definitions or of the value of ΔE in the limit of an infinite number of degrees of freedom.

Classic heuristic arguments using the daemon energy lead to misleading conclusions, for instance in the case of negative-temperature systems. For this reason we prefer not to use this concept at all. We notice, moreover, that the daemon concept is actually not useful as its energy contains no more information than the state energy $\mathscr{E}$.

3.1. Definition of Creutz's algorithm

We consider an ensemble of states of a physical system. Each state x is a set of M values, $x = (x_i)_{1 \leq i \leq M}$. The set of states

$$X = \{x = (x_i)_{1 \leq i \leq M}\} \tag{24}$$

is called the *configuration space*. Note that $i \in \mathbb{N}$ is the index for components of x.

For instance, a state of an Ising spin system is given by $\forall i \; x_i \in \{-\frac{1}{2}, +\frac{1}{2}\}$. Note that the values x could also be continuous, i.e. $\forall i \; x_i \in \mathbb{R}$. For the 2D Euler equations, the configuration space is X_N as defined in equation (8), and $M = N^2$.

The energy of each microstate is given by $\mathscr{E}(x)$. Furthermore, we define

$$\Gamma(E_0, \Delta E) = \{x \in X \mid E_0 \leq \mathscr{E}(x) \leq E_0 + \Delta E\} \tag{25}$$

as the set of microstates in the energy shell $E_0 \leq \mathscr{E}(x) \leq E_0 + \Delta E$. The microcanonical measure is defined as the uniform measure over $\Gamma(E_0, \Delta E)$ (each microstate in $\Gamma(E_0, \Delta E)$ has probability $\Omega(E, \Delta E) = (\#\Gamma(E_0, \Delta E))^{-1}$ to occur, where we recall that $\#(A)$ is the cardinality of set A). Furthermore, as in section 3, we assume that $\Delta_M E \ll \Delta E \ll E_0$. Our goal is to sample the microcanonical measure over $\Gamma(E_0, \Delta E)$.

We assume that there exists a Markov chain $\mathscr{T}$, defined through a sequence of random numbers $\{y^l \in X\}_{l \geq 0}$ with *transition probability* $T(x, x')$ (so $T(x, x')$ is the probability to observe $y^{l+1} = x$ if $y^l = x'$). Here, $l \in \mathbb{N}$ is the index for the position in the Markov chain. We assume that $\mathscr{T}$ verifies detailed balance for the uniform measure on X. This is equivalent to the statement $T(x, x') = T(x', x)$. See appendix A for more details. Lastly, we note that $\mathscr{T}$ (or T) does not depend on the system energy.

In order to sample the microcanonical measure over $\Gamma(E_0, \Delta E)$ an algorithm is needed that generates realizations $\{z^l\}$ of a new Markov chain $\mathscr{Q}$ defined by its corresponding transition probability Q and over the configuration space $\Gamma(E_0, \Delta E)$. We shall call this algorithm Creutz's algorithm, and we define it in the following way.

Let the system's current state be $y^l = x'$. We pick at random $x \in X$ with probability $T(x, x')$. If $E_0 \leq \mathscr{E}(x) \leq E_0 + \Delta E$ then we accept this move and $y^{l+1} = x$. Otherwise, we do not accept and $y^{l+1} = y^l = x'$. Iteration of this procedure defines a Markov chain $\mathscr{Q}$.

We can show that Q verifies detailed balance for the uniform measure over $\Gamma(E_0, \Delta E)$. It is easily checked that $Q(x, x') = T(x, x')$ if $x \neq x'$, and $Q(x, x) = T(x, x) + \sum_{x' \in X \backslash \Gamma(E, \Delta E)} T(x', x) = 1 - \sum_{x' \in \Gamma(E_0, \Delta E), x \neq x'} T(x, x')$. ($Q(x, x)$ is the probability of a move from y^l to y^{l+1} to fail because of the energy constraint.) We thus find that $\forall x, x' \in \Gamma(E_0, \Delta E): Q(x, x') = Q(x', x)$ by virtue of the detailed balance on $\mathscr{T}$. Therefore, $\mathscr{Q}$ verifies a detailed balance for a uniform measure on $\Gamma(E_0, \Delta E)$. Thus, $\mathscr{Q}$ has this uniform measure as a stationary measure, see appendix A. In conclusion, if $\mathscr{Q}$ is ergodic then it samples the microcanonical measure over $\Gamma(E_0, \Delta E)$.

We conclude by describing how to properly empirically sample an observable A. The expectation value of observable A is computed through

$$\langle A(y) \rangle = \lim_{N \to \infty} \frac{1}{L} \sum_{l=1}^{L} A(y^l). \tag{26}$$

It is important to notice that if for y^l, the Creutz algorithm fails to change the state K times ($y^l = y^{l+1} = \cdots y^{l+K-1}$), then these K configurations need to be included into the sum (26). We clarify this statement in appendix B.

3.2. Temperature computation using the Creutz algorithm

We continue with the computation of the inverse temperature from the energy distribution at equilibrium. We denote $\rho_M(E)$ as the density of states for energy E. The number of microstates in $\Gamma(E_0, \Delta E)$ then reads

$$\Omega_M(E_0, \Delta E) = \int_{E_0}^{E_0 + \Delta E} \mathrm{d}E \, \rho_M(E). \tag{27}$$

We assume that the energy density of states has a large-deviation behavior, i.e.,

$$\forall E \quad \lim_{M \to \infty} \frac{1}{M} \log \rho_M(E) \underset{M \to \infty}{\to} S(E). \tag{28}$$

We can assume a stronger property, namely

$$\rho_M(E) \underset{M \to \infty}{\sim} C(E) \, \mathrm{e}^{MS(E)}. \tag{29}$$

We note that this assumption is verified for most microcanonical measures. For the 2D Euler equations, it follows from the large-deviation results discussed in section 2.3.

In the microcanonical ensemble the temperature is defined as $\beta = \mathrm{d}S/\mathrm{d}E$. It then follows that $S(E) = S(E_0) + \beta(E - E_0) + o(E - E_0)$ and $\rho_M(E) \underset{M \to \infty}{\sim} C(E)\mathrm{e}^{MS(E_0)+\beta M(E-E_0)}$. We thus have, using the fact that equation (27) is a Laplace integral, that $\lim_{M \to \infty}(1/M) \log \Omega_M(E_0, \Delta E) = S(E_0)$ is independent of ΔE.

Moreover,

$$\rho_M(E) \underset{M \to \infty}{\sim} C_1(E_0, \Delta E) \, \mathrm{e}^{-\beta M(E-E_0)}, \tag{30}$$

and

$$P(E) \underset{M \to \infty}{\sim} C_2(E_0, \Delta E) \, \mathrm{e}^{-\beta M(E-E_0)}. \tag{31}$$

The energy distribution is exponential with rate βM. If β is positive, the energy of the system is concentrated close to $E_0 + \Delta E$. If β is negative, the energy of the system is concentrated close to E_0.

We will return to this result in section 4.

3.3. 2D Euler algorithm

We now want to apply the Creutz algorithm to the 2D Euler model. We will follow the general definition from section 3.1. Thus, we need to (i) define a Markov chain for the

2D Euler model and (ii) precisely define the approximate energy such that we can sample states in the energy shell $[E_0, E_0 + \Delta E]$.

Firstly, following section 3.1, we consider the Markov chain $\mathscr{T}$, now defined through its configuration space

$$X_N = \left\{ \omega^N = (\omega_{ij})_{0 \leq i,j \leq N-1} \mid \forall i,j \; \omega_{ij}^N \in \{\sigma_1, \ldots, \sigma_n\} , \qquad \text{and} \right.$$
$$\left. \forall k \; \# \left\{ \omega_{ij}^N \mid \omega_{ij}^N = \sigma_k \right\} = N^2 A_k \right\}, \tag{32}$$

and transition probability $T(\omega, \omega')$. T denotes the probability to go from a vorticity state $y^l = \omega' \in X_N$ to $y^{l+1} = \omega \in X_N$, where as before $l \geq 0$ denotes the position of y^l in $\mathscr{T}$. We assume the detailed balance condition holds for $\mathscr{T}$.

Secondly, we need to calculate the approximate energy $\mathscr{E}_N$ given by equation (10). The discretized vorticity field ω^N is transformed to Fourier space with a two-dimensional (discrete) fast Fourier transform (FFT). The discretized velocity field and stream function field are then computed by making use of the Fourier representation of equations (1) and an inverse FFT, resulting in $\mathbf{v}^N = (\mathbf{v}_{ij}^N)_{0 \leq i,j \leq N-1}$ and $\psi^N = (\psi_{ij}^N)_{0 \leq i,j \leq N-1}$.

With these definitions the microcanonical measure over equation (9) can be sampled. We take the current system state to be $y^l = \omega \in X_N$ (the current vorticity-field configuration) and $y^{l+1} = \omega \in X_N$ as the next state (next vorticity-field configuration) in $\mathscr{T}$. Similarly, the current energy is denoted by $\mathscr{E}_N[y^l]$ and the energy of the next state by $\mathscr{E}_N[y^{l+1}]$.

We now describe how we construct a realization of the Markov chain $\mathscr{T}$ under the energy constraint. The vorticity field $y^0 = \omega^N \in X_N$ is initialized with $N^2/2$ values of $\sigma_+ = +1$ and $N^2/2$ values of $\sigma_- = -1$ such that the conditions $\sum_{k=1}^{2} A_k = 1$ and $\sum_{i,j=0}^{N-1} \omega_{ij}^N = 0$ are satisfied (see section 2.1). We use a two-level potential vorticity distribution as an example, but generalization to higher-level distributions is straightforward. To sample the microcanonical measure, obeying the energy and vorticity distribution constraints, the following routine is followed.

(1) Let the current state of the system be $y^l = \omega'$. We randomly choose two lattice sites, (i_0, j_0) and (i_1, j_1), with a uniform distribution. The values at these sites are $\omega'_{i_0 j_0}$ and $\omega'_{i_1 j_1}$, respectively. The vorticity values at these positions are then interchanged. In other words, $\omega_{ij} = \omega'_{ij} \; \forall ij \neq \{i_0 j_0, i_1 j_1\}$, $\omega_{i_0 j_0} = \omega'_{i_1 j_1}$, and $\omega_{i_1 j_1} = \omega'_{i_0 j_0}$. We note that by interchanging two vorticity values, the new field ω still belongs to X_N.

(2) The new energy, $\mathscr{E}_N[\omega^N]$, is calculated.

(3) The energy check is performed. If $E_0 \leq \mathscr{E}_N[\omega^N] \leq E_0 + \Delta E$ then we accept the move in step (1), i.e., $\omega^{l+1} = \omega$. If the new energy is not in the allowed energy range, we reverse step (1) such that we get the old vorticity field back, i.e., $\omega^{l+1} = \omega^l = \omega'$. The new energy in this case is thus given by $\mathscr{E}_N[\omega] = \mathscr{E}_N[\omega']$. This step ensures conservation of energy and only configurations that are in the set $\Gamma_N(E_0, \Delta E)$ are allowed, see equation (9). In either case, we return to step (1).

Iteration of steps ((1)–(3)) then builds a realization $\{\omega^l\}_{l \geq 0}$ of the Markov chain Q. Since we assumed that detailed balance holds for $\mathscr{T}$, we know (by virtue of section 3.1) that the microcanonical measure is an invariant measure of Q. If we assume Q to be ergodic then we sample the microcanonical measure.

This vorticity exchange method has some analogies with spin ones in the Kawasaki algorithm [30]. The Kawasaki algorithm is a convenient way to treat dynamics with

14

conservation laws in spin or lattice gas Monte Carlo dynamics. Our algorithm slightly differs from Kawasaki's, as we consider non-local vorticity value exchanges.

We define a Monte Carlo step as N^2 accepted changes in the vorticity field, for reasons mentioned in section 3.1. Typically, equilibrium is reached after ten Monte Carlo steps for a two-level distribution and fifty for a three-level vorticity distribution. We note that the equilibration time depends on the energy E_0 chosen.

4. Numerical results

In this section we present the numerical results obtained by sampling the microcanonical measure of the 2D Euler equations using the algorithm described in section 3.3. For pedagogical reasons, we restrict the simulations to two- and three-level vorticity distributions, but note that generalization to more general vorticity-level distributions is straightforward. We consider the vorticity distribution (see equation (7))

$$D(\sigma) = \tfrac{1}{2}\,\delta(\sigma - \sigma_+) + \tfrac{1}{2}\,\delta(\sigma - \sigma_-) \tag{33}$$

for the two-level distribution, and

$$D(\sigma) = \tfrac{1}{4}\delta(\sigma - \sigma_+) + \tfrac{1}{2}\delta(\sigma - \sigma_0) + \tfrac{1}{4}\delta(\sigma - \sigma_-) \tag{34}$$

for the three-level distribution. In the above, $\sigma_+ = 1$, $\sigma_0 = 0$, $\sigma_- = -1$.

4.1. Mean-field behavior and negative temperature

4.1.1. Mean-field predictions. The variational problems (23) associated to the two- and three-level cases have been explicitly solved in the past, see [24, 25, 31]. We summarize their results here and compare them to our numerical results.

For the two-level vorticity case the local probability to find a vorticity value of $\omega = \sigma_+ = 1$ is found to be $\rho_1 = \tfrac{1}{2}(1 - \tanh(\alpha - \beta\psi(\mathbf{r})))$ [5], where α and β are Lagrange parameters associated with the conservation of area A and energy, respectively. Furthermore, β is the inverse temperature, $\beta = \mathrm{d}S/\mathrm{d}E$. Since there are only two possible values for ω, the local probability to find a vorticity value of $\omega = \sigma_- = -1$ is therefore $\rho_2 = 1 - \rho_1$. Hence, the locally averaged vorticity reads

$$\overline{\omega} = \rho_1\sigma_+ + (1 - \rho_1)\sigma_- = -\tanh(\alpha - \beta\psi). \tag{35}$$

We consider a symmetric distribution $D(\sigma)$ $(D(\sigma) = -D(-\sigma))$. If we assume this symmetry then $\alpha = 0$.

For the three-level distribution a similar calculation, assuming symmetry is not broken, yields [31]

$$\overline{\omega} = \frac{\mu \sinh(\beta\psi)}{1 + \mu \cosh(\beta\psi)}, \tag{36}$$

where μ is an additional Lagrange parameter arising from the conservation of A.

4.1.2. Negative temperature in doubly periodic domains. The first statistical mechanics approach to self-organization of 2D turbulence was Onsager's work on the point vortex model [32]. Onsager argued in his paper that ensembles of point vortices may have negative

temperatures. This property is traced back to the fact that, in contrast with many other systems, the phase space is bounded (the point vortex model has no quantity analogous to the kinetic energy in particle systems, allowing the system to explore higher and higher energy with increasing entropy). The same argument also holds for the 2D Euler equations with continuous vorticity fields, so one expects negative temperatures to exist for some ranges of energy. In this section we show that, in the case of a doubly periodic domain, the inverse temperature of the 2D Euler equations is actually always negative. Note that the proof was first established by Mikelic and Robert [33].

From the mean-field variational problem we can prove that for any vorticity distribution there exist functions f such that

$$\omega = \Delta\psi = f(\beta\psi). \tag{37}$$

Moreover, it can be proven that $f'(x) > 0$ (see for instance [5]).

Multiplying the above equation by $\Delta\psi$ and integrating by parts gives

$$\beta = -\frac{\int_{\mathscr{D}} \mathrm{d}^2\mathbf{r}\,(\Delta\psi)^2}{\int_{\mathscr{D}} \mathrm{d}^2\mathbf{r}\,(\nabla\psi)^2\,f'(\beta\psi)}. \tag{38}$$

Using $f'(x) > 0$, we conclude that[3] $\beta < 0$.

Let us find the value of β in the low energy limit for domain $\mathscr{D}$. Previous works [1] have shown that in this limit, the expression for the vorticity field for the parallel flow is given by $\omega = A\cos(2\pi x + \phi)$ (or $\omega = A\cos(2\pi y + \phi)$), where A is a constant depending on E and ϕ is an arbitrary phase. Furthermore, in the same limit, we may linearize equation (37) and find $\omega \simeq \beta\psi$. From $\omega = A\cos(2\pi x + \phi) = \Delta\psi$ we compute $\psi = -(4\pi^2)^{-1}\omega$. Together with $\omega \simeq \beta\psi$ we find that $\beta = -4\pi^2$, which is indeed negative for all energies.

4.1.3. Numerical results. We now confront the analytical results with numerical computations. In order to do so, we must first ensure that the system is in equilibrium. We can test this by computing the mean-field entropy. We recall the entropy of a coarse-grained macrostate p^N, see equation (19). The mean-field entropy is computed for the two-level distribution ($K = 2, \sigma_+ = 1, \sigma_- = -1$) with parameter values $N = 256$ and $n = 3$, and energies ranging from $E_0 = 0.01E_{\max}$ to $0.99E_{\max}$. Here, $E_{\max}$ is the maximum possible value of energy that the two-level system can obtain. We will compute $E_{\max}$ below. We take $\Delta E = 0.01E_0$ but note that its value is not of high importance since the actual energy fluctuations at this resolution are much lower than ΔE.

The result is depicted in figure 1(a). Equilibrium is reached quickly for all energy levels. To be on the safe side, we take an equilibration time of one hundred Monte Carlo steps. We define a Monte Carlo step as M accepted iterations of the Creutz algorithm. With this definition, the size of a state x and the Monte Carlo step scale linearly, such that after K Monte Carlo steps each value x_i has been changed K times on average. All results that follow below were obtained after the system had reached equilibrium.

Two-level vorticity distribution. For the 2D Euler equations and for a given vorticity distribution, energy maxima correspond to segregated states. For example, when the left half of the vorticity field contains only values of $\sigma_+ = 1$ and the right half consists solely values of $\sigma_{-1} = -1$ we have $E_0 = E_{\max}$.

---

[3] Note that doubly periodicity is required to ensure that the temperature is always negative. This is due to a partial integration step in the proof.
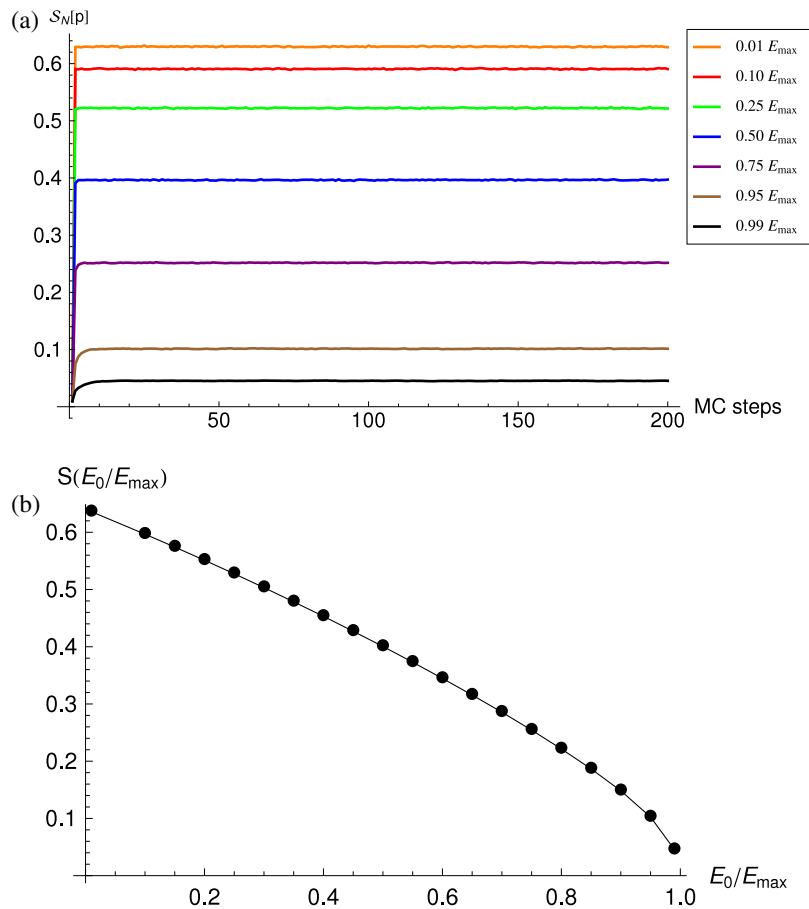
Figure 1. (a) Mean-field entropy as a function of Monte Carlo steps for a two-level vorticity distribution at a resolution of $N = 256$. Equilibrium is reached within fifty Monte Carlo steps for any energy level. (b) Mean-field entropy as a function of $E_0/E_{\max}$. The numerical fluctuations are smaller than the size of the balls.

We calculate $E_{\max}$ analytically. We have $\mathrm{d}^2\psi/\mathrm{d}x^2 = -1$ for $0 \leq x < \frac{1}{2}$ and $\mathrm{d}^2\psi/\mathrm{d}^2x = +1$ for $\frac{1}{2} \leq x < 1$. The general solutions to these two differential equations on their respective domains are denoted by ψ_{-1} and ψ_1. These equations are complemented with the boundary conditions $\psi_{-1}(0) = \psi_1(1) = 0$, $\psi_{-1}(\frac{1}{2}) = \psi_1(\frac{1}{2})$, and $\psi'_{-1}(\frac{1}{2}) = \psi'_1(\frac{1}{2})$. We find $\psi_{-1}(x) = -x^2/2 + \frac{1}{4}x$ and $\psi_1(x) = x^2/2 - \frac{3}{4}x + \frac{1}{4}$. The maximum energy is now easily calculated as $E_{\max} = \frac{1}{96}$. The numerical value of $E_{\max} = 0.0104$ corresponds well to this theoretical value.

We perform numerical simulations at $N = 256$ for $E_0 = 0.9 E_{\mathrm{Max}}$ and an energy tolerance set to $\Delta E = 0.01 E_0$. After reaching equilibrium, we compute the p^N and stream function ψ^N by point-wise averaging one hundred fields that are separated in time by N^2 permutations, respectively. The averaged coarse-grained vorticity field $\bar{\omega}^N$ is then computed from p^N. Figure 2(a) shows the averaged coarse-grained vorticity $\bar{\omega}^N$ versus the averaged stream function ψ^N.

The data points (blue) are fitted with equation (35) by tuning the Lagrange parameter β. The result (red curve) corresponds to a temperature of $\beta = -96.2$. The numerical results
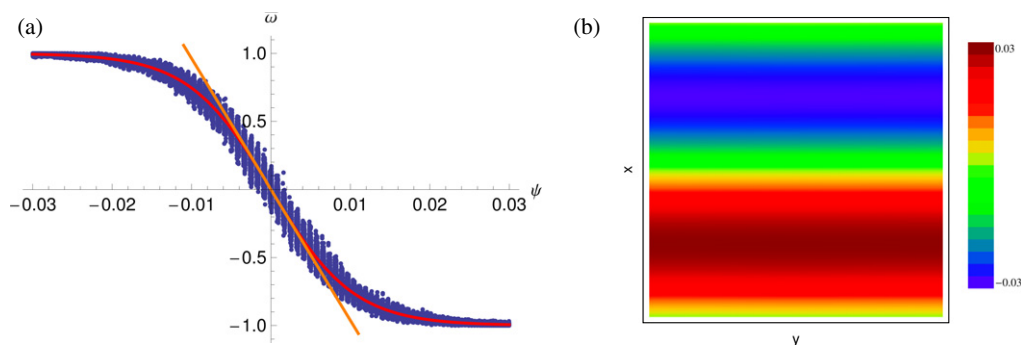
Figure 2. Numerical result of a two-level vorticity distribution with resolution 256×256 at energy $E_0 = 0.90E_{\max}$ and coarse-graining parameter $n = 3$. (a) Averaged coarse-grained vorticity versus stream function. An inverse temperature of $\beta = -96.2$ is found. (b) The averaged stream function field shows a parallel (pure) flow.

are clearly in agreement with the theoretical predictions. In figure 2(b) the stream function field is plotted, showing a unidirectional flow.

The fluctuations in $\bar{\omega}^N$ visible in figure 2(a) are a result of the coarse graining of ω (or equivalently in p). The level of fluctuations in p^N is of $o(1/\sqrt{n^2}) = o(1/n)$. This amounts to fluctuations of about 0.3 for $n = 3$. This is close to the observed fluctuations near the center ($\psi = 0$), see figure 2(a).

Three-level vorticity distribution. Although determining $E_{\max}$ for the two-level case was possible due to the simple geometry, this is less trivial for the three-level case. Instead of trying to compute $E_{\max}$ analytically, we determine it numerically. We let the algorithm run for some time and accept only moves that increase the energy. We find that the system converges towards a maximum energy of $E_{\max} = 0.005\,208$.

We now show results for a three-level distribution with $N = 256$, $E_0 = 0.9E_{\max}$ and an energy tolerance of $\Delta E = 0.01E_0$. We follow the same averaging procedure as in the two-level case, see above.

In figure 3(a) the averaged coarse-grained vorticity $\bar{\omega}^N$ is plotted against the averaged stream function ψ^N. The data points (blue) are fitted with equation (36), see figure 3 for more details. This is again in agreement with theory. In figure 3(b) the averaged stream function field is plotted, showing a dipole flow.

4.2. Inverse temperature computation

The 2D Euler equations have the property of negative temperature, as discussed in section 4.1.2.

In this section we present three different methods to compute the inverse temperature of the two-level vorticity system. The first method is a direct measure of energy fluctuations, as discussed in section 4.2.1. It is independent of any assumption (mean field, large N, etc). It is therefore a good method to verify the two other methods which rely on mean-field approximations. The second method, studied in section 4.2.2, uses the mean-field equation (35) and a fit to compute β. The third method, proposed in
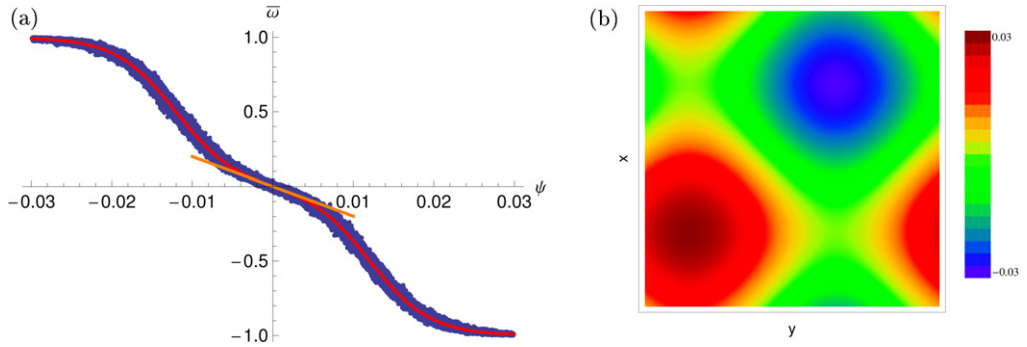
Figure 3. Numerical result of a three-level vorticity distribution with resolution 256×256 at energy $E_0 = 0.9E_{\max}$ and coarse-graining parameter $n = 3$. (a) Averaged coarse-grained vorticity versus stream function. The fitting parameters are $\beta = -252.1$ and $\mu = 0.0969$. (b) The averaged stream function field shows a dipole flow.

section 4.2.3, uses the mean-field approximation of the entropy (22) to find β from the relation $\beta = \mathrm{d}S/\mathrm{d}E$.

We show that all three methods give similar results. Furthermore, we find negative temperatures for all energies, in agreement with our finding in section 4.1.2.

Lastly, in the high energy limit, we find that the inverse temperature tends to $\beta = -\infty$. In the low energy limit, we find $\beta = -39.74$, which is close to the theoretically predicted value of $\beta = -4\pi^2$ for our domain $\mathscr{D}$, see section 4.1.2.

4.2.1. Temperature from the energy distribution in the Creutz algorithm. This method makes use of the theory discussed in section 3.2 and is applied to the two-level case.

After equilibrium is reached, the system's energy is computed ten times per Monte Carlo step for a total of one hundred Monte Carlo steps. The histogram is shown in figure 4(a) for $E_0 = 0.95E_{\max}$. The data are fitted with equation (30), from which we obtain a value of β.

This method is repeated for different values of energy E_0, such that we obtain a plot of β versus energy, as shown in figure 4(b). Notice that the temperature is negative over the full range of energy values, as expected.

4.2.2. Temperature from the mean-field equation. We compute the inverse temperature through the mean-field equation (16) by using the same method as discussed in section 4.1.1, see also figure 2(a).

After the system has reached equilibrium, the average fields ψ^N and $\bar{\omega}^N$ are computed for several energies E_0. We plot $\bar{\omega}^N$ versus ψ^N for each energy and fit the result with equation (35) from which we obtain a negative temperature $\beta(E)$, see the red curve in figure 5.

4.2.3. Temperature from the mean-field entropy. This method relies on the mean-field entropy, see equation (22) and section 4.1.1.

For each chosen energy E_0 the algorithm is run until equilibrium is reached. The simulation is then continued for another fifty Monte Carlo steps. We average the coarse-
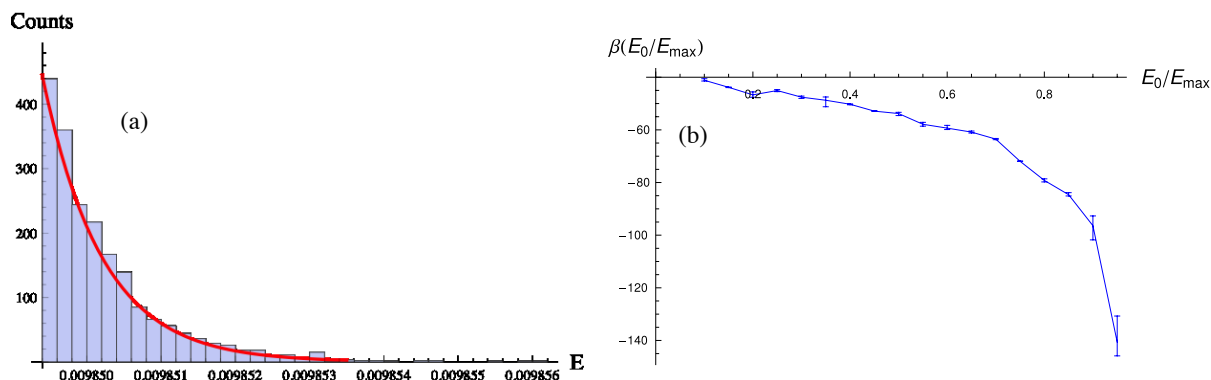
Figure 4. Two-level vorticity distribution with $N = 256$. (a) The energy distribution after reaching equilibrium. The energy distribution is proportional to $\Omega_N(E)$. The distribution follows an exponential law (equation (30)), see the red curve. This gives access to the inverse temperature β. (b) The inverse temperature, obtained using the method of (a), is plotted for several energies E_0. The error bars show the standard error of the estimate of β obtained via the fitting procedure.
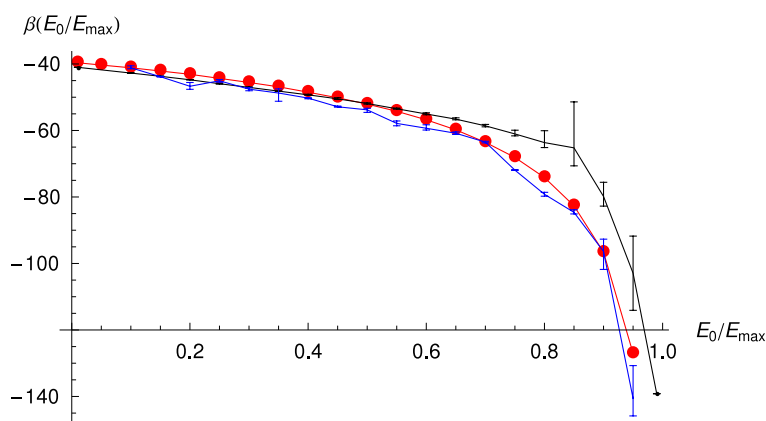

Figure 5. Inverse temperature plotted against energy from the equilibrium energy distribution (blue), the mean-field equation (red) and the mean-field entropy (black).

grained entropy and energy over this interval and repeat this process for energies ranging from $E_0 = 0$ to $E_{\max}$. The data are fitted with a polynomial, which can be derived. The temperature of the system is then found via $\beta(E) = \mathrm{d}S/\mathrm{d}E(E)$. The resulting values of β are then plotted against energy, see the black curve in figure 5.

From the same figure we can conclude that the temperature is indeed negative for all values of E_0. Furthermore, note that all three methods give very similar results, especially in the low energy limit. In this limit, statistical mechanics theory predicts a temperature of $\beta = -4\pi^2$, see section 4.1.2. The values in this limit, shown in the figure, indeed approach this theoretical value.

5. Phase transitions and statistical ensemble inequivalence

In this section, we use Creutz's algorithm in order to study the microcanonical measures for the 2D Euler equations. We are specifically interested in the study of phase transitions, as they play a major role in the dynamics of equilibrium and non-equilibrium flows [7, 1]. The numerical computations shown in this section are compared with the low energy statistical equilibria and phase diagrams analytically computed in [7, 1]. Creutz's algorithm allows us to search beyond the low energy limit. In section 5.2, we observe a first-order phase transition that does not exist in the low energy limit, for a three-level vorticity distribution.

5.1. Summary of theoretical results

We begin with a summary of the theoretical results describing phase transitions for the 2D Euler equations in the low energy limit [1, 34]. In a domain with doubly periodic boundary conditions and in the low energy limit, statistical equilibria are well approximated by largest scale eigenmodes of the Laplacian

$$\omega(x,y) \underset{E \to 0}{\sim} A \cos(2\pi x + \phi) + B \cos(2\pi y + \phi'), \tag{39}$$

where A, B are constants.

For a square geometry, there are three possible equilibrium flows. Two of these equilibria have amplitudes of $(A = 0, B \neq 0)$ and $(A \neq 0, B = 0)$, respectively, and are called pure states, or parallel flows. The last type of flow, called a symmetric dipole, is the case for which $A = B$. Symmetric dipoles and parallel flows have been found numerically with our algorithm, see the previous sections. We proceed now to a more detailed study of the phase transitions between these equilibria when the energy is changed.

It is shown in [1, 34] that the selection of either a dipole or a parallel flow in the low energy limit is related to inflection points in the relation between the coarse-grained vorticity and the stream function. To be more precise, consider the Taylor expansion

$$\omega = f(\beta\psi) \qquad \text{with } f(x) = x + a_4 x^3 + o(x^3). \tag{40}$$

Using $\beta < 0$ (see section 4.1.2), we note that when $a_4 > 0$, the curve $\omega - \psi$ bends upwards for positive x, similar to a hyperbolic sine. When $a_4 < 0$, then it bends downward for positive x, similarly to a hyperbolic tangent. The theory predicts parallel flows when $a_4 < 0$, and dipole flows when $a_4 > 0$.

Let us study this criterion in the case of a two-level vorticity distribution. From the theoretical predictions (equation (35)) we find for the two-level case with symmetric vorticity distribution ($\alpha = 0$) that $\omega \simeq \beta\psi - \frac{1}{3}\beta^3\psi^3$, from which we find that $a_4 = -\frac{1}{3} < 0$, in accordance with the tanh-like behavior observed (see figure 2(a)). We thus expect to always observe parallel flows for the two-level case, and no phase transitions. This is in agreement with the results obtained by using Creutz's algorithm.

The three-level case is more interesting. Linearization of equation (36) yields $\omega \simeq (\mu/(1+\mu))\beta\psi + ((1-2\mu)\mu/6(1+\mu)^2)\beta^3\psi^3$. For $0 \leq \mu < 1/2$ we find that $a_4 > 0$ and expect to observe a dipole. This is the case studied in the previous section (see figure 3). Interestingly, in the three-level case, $a_4(\mu) = (1-2\mu)\mu/6(1+\mu)^2$ is negative for either $\mu > 1/2$ or $\mu < 0$. This open the possibility of a phase transition in the three-level case.

We have not tried to theoretically compute μ as a function of the energy as this would be very involved, but we find that a phase transition actually exists using Creutz's algorithm. We show the result in section 5.2.

The theoretical results [1, 34] are valid in the low energy limit. In this limit the theoretical results indicate that the transition is of second order (symmetry breaking, by transition from parallel to dipole flows) and occurs when $a_4 = 0$. In the following we perform computations both in the low energy limit and for large energies. We find that the sign of a_4 remains relevant for finding phase transitions. However, we will see that for large energies the transition can be of first order.

5.2. Phase transition in the three-level case

In order to study the phase transition between dipole and parallel flows we first define an appropriate order parameter. We consider the Fourier coefficients of the vorticity field ω^N, denoted $\hat{\omega}_{\mathbf{k}}$, where $\mathbf{k} = (k_x, k_y)$, such that in equation (39) $A = |\hat{\omega}_{(2\pi,0)}|$ and $B = |\hat{\omega}_{(0,2\pi)}|$. We define $\omega_{\min} = \min\left\{|\hat{\omega}_{(2\pi,0)}|, |\hat{\omega}_{(0,2\pi)}|\right\}$ and $\omega_{\max} = \max\{|\hat{\omega}_{(2\pi,0)}|, |\hat{\omega}_{(0,2\pi)}|\}$. Then the order parameter

$$r = \frac{\omega_{\min}}{\omega_{\max}} \tag{41}$$

characterizes the equilibrium state in which the system resides. We have $0 \leq r \leq 1$, and for $r = 1$, $\omega_{\min} = \omega_{\max}$, $A = B$ and we observe a purely symmetric dipole, whereas for $r = 0$, $\omega_{\min} = 0$, we find that either A or B is equal to zero, corresponding to either a horizontal or a vertical parallel flow. For an intermediate value of r, a mixed state between a parallel flow and a dipole will be observed (which is not a statistical equilibrium but can be observed transiently).

For $N = 128$ we compute the order parameter 256 times per Monte Carlo step for energies ranging from $E_0 = 0$ to $E_{\max}$ for the two- and three-level cases, see figure 4. For both cases we found degeneracy at very low energies. Indeed, in a square box, theory [7, 1] predicts a second-order phase transition at $E = 0$ as $a_4 \underset{E \to 0}{\to} 0$. Then, for finite N, both parallel and dipole flows are possible at non-zero but small energies due to finite-size effects. Figure 4(a) confirms this. It is also expected in [7, 1] that there is no other phase transition for $E > 0$ in the case of two levels of vorticity. Our numerical results agree with this observation.

For the three-level case, figure 6(b) shows that a phase transition exists around $E_0 = 0.7E_{\max}$.

In order to determine the order of the phase transition, we ran Creutz's algorithm with three levels of vorticity, increasing the energy adiabatically from $E_m = 0.60E_{\max}$ up to $E_M = 0.82E_{\max}$; see figure 7. We took a resolution of $N = 256$ such that the fluctuations were small.

Two simulations were run at this resolution: a forward (low to high energy) simulation and a backward (high to low energy) simulation. The energy is adiabatically increased (decreased) with a rate corresponding to $4.4 \times 10^{-4}E_{\max}$ per Monte Carlo step, for a total of 500 Monte Carlo steps. Within each Monte Carlo step, we compute averages of the order parameter over 512 realizations, for each of the 500 energy levels. The result is shown in figure 7. We observe hysteresis behavior, a typical signature of first-order phase transitions.
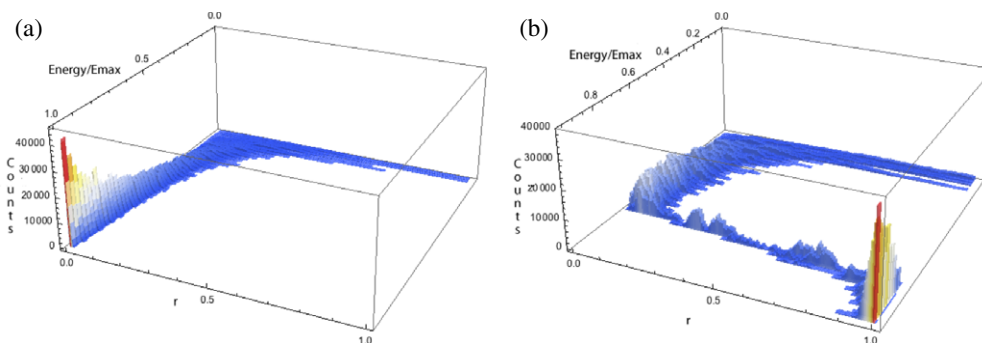
Figure 6. The order parameter r versus $E/E_{\max} = 0$ to $E/E_{\max} = 1.0$ for two-level (a) and three-level (b) vorticity distributions. Both distributions show degeneracy at low energies. Only the three-level case exhibits a phase transition around $E = 0.7 E_{\max}$.
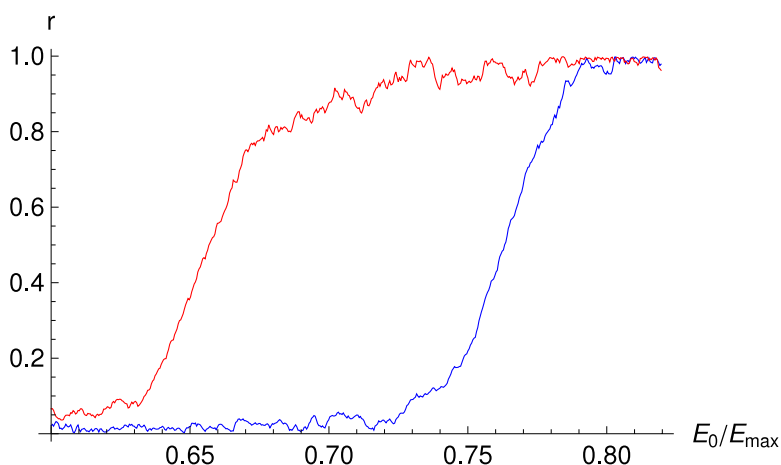

Figure 7. Hysteresis in the transition from parallel flow to dipole. The plot shows the order parameter versus the energy for a forward (low to high energy) simulation (blue) and a backward (high to low energy) simulation (red) (resolution $N = 256$).

Using the standard terminology in describing phase transitions, the dipole is the ordered phase in the sense that it has lost the translational symmetry. The parallel flow is the corresponding disordered phase. An interesting remark is that we observe a transition from the disordered phase to the ordered one as the energy is increased. This is in contrast with classical thermodynamics and statistical physics results. For instance, the first-order solid–liquid transition is a transition from the ordered phase (solid with broken symmetry) to the disordered phase (liquid) when the energy (or temperature) is increased. Similarly, the ferromagnetic–paramagnetic phase transition is a second-order phase transition from the ordered phase (ferromagnetism, with broken symmetry) to a disordered phase (paramagnetism) when the energy is increased.

This paradox is due to the fact that our system has a negative temperature. Then the entropy decreases with the energy. It is thus natural to expect a transition from the disordered state (high entropy and symmetric) to the disordered state (low entropy and with broken symmetry) when the energy is increased. This paradoxical property is traced

back to the fact that, in contrast with any other systems, for the 2D Euler equations the phase space is bounded (there is no equivalent of kinetic energy allowing the system to explore higher and higher energy with increasing entropy).

We have described a first-order phase transition in the microcanonical ensemble with hysteretical behavior. In systems with short-range interactions, microcanonical first-order transitions usually do not exist because of the possibility of phase coexistence [8], whereas they are generic features in systems like the 2D Euler equations which have long-range interactions. A very general argument [8] shows that such a first-order phase transition in the microcanonical ensemble is necessarily associated with a situation of inequivalence between the microcanonical and canonical ensembles.

6. Conclusions

In this paper we have presented a novel numerical method based on Creutz's algorithm to sample microcanonical measures of hydrodynamical systems. Although we have only presented numerical results for the 2D Euler model, we stress that this numerical scheme can easily be generalized to more complex hydrodynamical models such as the axisymmetric 3D Euler equations or the shallow water equations.

For the 2D Euler model, we have reproduced the (theoretically) well-known equilibrium states characterized by parallel and dipole flows. Using our algorithm, we were able to compute the temperature of the system in three different ways. One of these approaches allowed the computation of the temperature without making use of any mean-field assumptions, and therefore served as a verification tool for the mean-field approximations made in theoretical predictions. All three methods match very well, showing consistency between the numerical approach and the mathematical results; this also proves that the mean-field description is exact in the large-N limit.

Furthermore, we have found a previously unknown phase transition in the microcanonical description of the 2D Euler equations. We have shown that in the energy range where the transition occurs there is an ensemble inequivalence between the microcanonical and canonical ensembles. This transition is very interesting from a statistical mechanics point of view, as it is a transition from an ordered phase with broken symmetry towards an asymmetric ordered phase when the energy is increased. From a fluid mechanics point of view, it is also very interesting, as it describes a discontinuous change of the flow topology. A similar phase transition has already been observed in a non-equilibrium framework for the 2D stochastic Navies–Stokes equations [7]. This new equilibrium result will probably be very useful in explaining why the 2D-Navier–Stokes non-equilibrium phase transition has the phenomenology of a first-order phase transition rather than of a second-order one.

The numerical method we propose is extremely easily implemented and the generalization to similar models is rather straightforward. We guess that it will have many applications for theoretical, experimental and geophysical flows.

Acknowledgments

Appendix A. Markov chains, detailed balance and invariant distributions

In this appendix we formalize the notions of Markov chain, detailed balance, and reversible Markov chain. These definitions are used in sections 3.1 and 3.3.

Markov chain. A Markov chain is a (mathematical or physical) system that undergoes changes from one state to another between a finite number of states. Such changes are called *transitions* and the probabilities associated with the state changes are called *transition probabilities*. The system is driven by a random and memoryless process, i.e., the next state in the chain depends only on the current state and not on the sequence of states that preceded it. The memoryless property of the system is usually referred to as the *Markov property*. The set of all possible states, called the *configuration space*, and the transition probabilities fully characterize a Markov chain.

The configuration space is defined by

$$X = \{x = (x_i)_{1 \leq i \leq M}\}.$$

A state is thus described by a set of M values, $x = (x_i)_{1 \leq i \leq M}$.

Formally, a Markov chain $\mathscr{T}$ is a sequence of random variables $\{y^l \in X\}_{l \geq 0}$ with the Markov property, where the transitions between states are determined by the transition probabilities

$$T(x^{l+1}, x^l, x^{l-1}, \ldots, x^0) = T(x^{l+1}, x^l) = T(x, x').$$

This gives the probability to go from a state $y^l = x'$ to the state $y^{l+1} = x$. We call a sequence $\{z^l\}_{l \geq 0}$ a *realization* of the Markov chain $\mathscr{T}$. Note that $i \in \mathbb{N}$ is the index for components of x, while $l \in \mathbb{N}$ is the index for the position in the Markov chain. Furthermore, we denote $P^l(x')$ as the probability for $y^l = x'$. The probability to observe the system in state $y^{l+1} = x$ is then given by $P^{l+1}(x) = \sum_{x' \in X} T(x, x') P^l(x')$. The *stationary distribution*, denoted P^∞, is defined such that $P^\infty(x) = \sum_{x' \in X} T(x, x') P^\infty(x')$. The stationary distribution is thus invariant under T.

Detailed balance. A Markov chain $\mathscr{T}$ is said to be *reversible* with respect to the distribution $P^\infty(x)$ if

$$\forall x, x' \in X \colon P^\infty(x) T(x, x') = P^\infty(x') T(x', x). \tag{A.1}$$

This condition is also known as the *detailed balance* condition. Summing equation (A.1) over x gives

$$\forall x' \in X \colon \sum_{x \in X} P^\infty(x') T(x, x') = \sum_{x \in X} P^\infty(x') T(x', x) = P^\infty \sum_{x \in X} T(x', x) = P^\infty(x'). \tag{A.2}$$

Hence, for reversible Markov chains, P^∞ is always a steady-state (stationary) distribution of $\mathscr{T}$. In the case where $P^\infty(x)$ is uniform over X, i.e. $P^\infty(x) = \text{cste}$, the detailed balance condition reduces to

$$\forall x, x' \in X \colon T(x, x') = T(x', x). \tag{A.3}$$

We thus find that if a Markov chain obeys detailed balance, there exists an invariant (stationary) distribution P^∞ over X.

Appendix B. A wrong way to define and use the Creutz algorithm

A common error in using the Creutz algorithm is to define y^{l+1} as the first accepted move after y^l with the condition $E_0 \leq \mathscr{E}_N(y^{l+1}) \leq E_0 + \Delta E$, thereby discarding any unaccepted state in the expectation value of an observable A, cf equation (26). We consider the Markov chain that corresponds to this wrong procedure and show that it does not verify detailed balance.

Let us define more precisely the wrong algorithm. Given any configuration, we randomly pick a new configuration y^{l+1} with probability $T(x, x')$. If $E_0 \leq \mathscr{E}_N(y^{l+1}) \leq E_0 + \Delta E$ we accept the move. If the condition is not satisfied we keep picking new values for y^{l+1} at random until the condition $E_0 \leq \mathscr{E}_N(x) \leq E_0 + \Delta E$ is fulfilled and then accept the move. This defines a Markov chain $\mathscr{R}$ with transition probability

$$R(x, x') = C(x')T(x, x'), \tag{B.2}$$

where $C(x') = \sum_{x \in \Gamma_N(E, \Delta E)} T(x, x')$ is called the acceptance ratio (depending on x' only).

The detailed balance condition would require $\forall x, x' \in \Gamma_N(E, \Delta E)$: $R(x, x') = R(x', x)$. This would only hold when $C(x') = C(x)$, but there is no reason for this to be true in general.

We now recall how to properly empirically sample an observable A. The expectation value of observable A is computed through

$$\langle A(y) \rangle = \lim_{L \to \infty} \frac{1}{L} \sum_{l=1}^{L} A(y^l). \tag{B.3}$$

In using the above defined wrong Creutz algorithm, the expectation value of A is calculated over $\mathscr{R}$. Since the detailed balance condition does not hold for this Markov chain, one does not sample a stationary measure.

References

[1] Bouchet F and Venaille A, *Statistical mechanics of two-dimensional and geophysical flows*, 2012 *Phys. Rep.* **515** 227
[2] Lim C and Nebus J, 2007 *Vorticity, Statistical Mechanics, and Monte Carlo Simulation* (Berlin: Springer)
[3] Majda A J and Wang X, 2006 *Nonlinear Dynamics and Statistical Theories for Basic Geophysical Flows* (Cambridge: Cambridge University Press)
[4] Lim C, Ding X and Nebus J, 2010 *Vortex Dynamics, Statistical Mechanics and Planetary Atmospheres* (Singapore: World Scientific)
[5] Bouchet F and Sommeria J, *Emergence of intense jets and jupiter's great red spot as maximum entropy structures*, 2002 *J. Fluid. Mech.* **464** 165
[6] Venaille A and Bouchet F, *Oceanic rings and jets as statistical equilibrium states*, 2011 *J. Phys. Oceanogr.* **41** 1860
[7] Bouchet F and Simonnet E, *Random changes of flow topology in two-dimensional and geophysical turbulence*, 2009 *Phys. Rev. Lett.* **102** 094504
[8] Bouchet F and Barre J, *Classification of phase transitions and ensemble in equivalence in systems with long range interactions*, 2005 *J. Stat. Phys.* **118** 1073
[9] Bouchet F, Gupta S and Mukamel D, *Thermodynamics and dynamics of systems with long-range interactions*, 2010 *Physica A* **389** 4389
[10] Campa A, Dauxois T and Ruffo S, *Statistical mechanics and dynamics of solvable models with long-range interactions*, 2009 *Phys. Rep.* **480** 57
[11] Chavanis P, *Phase transitions in self-gravitating systems*, 2006 *Int. J. Mod. Phys.* B **20** 3113
[12] Ellis R S, Haven K and Turkington B, *Large deviation principles and complete equivalence and nonequivalence results for pure and mixed ensembles*, 2000 *J. Stat. Phys.* **101** 999

[13] Bouchet F, *Simpler variation problems for statistical equilibria of the 2d Euler equation and other systems with long-range interactions*, 2008 *Physica D* **237** 1976

[14] Creutz M, *Microcanonical Monte Carlo simulation*, 1983 *Phys. Rev. Lett.* **50** 1411

[15] Mukamel D, Ruffo S and Schreiber N, *Breaking of ergodicity and long relaxation times in systems with long-range interactions*, 2005 *Phys. Rev. Lett.* **95** 240604

[16] Gupta S and Mukamel D, *Relaxation dynamics of stochastic long-range interacting systems*, 2010 *J. Stat. Mech.* P08026

[17] Michel J and Robert R, *Large deviations for young measures and statistical mechanics of infinite-dimensional dynamical systems with conservation laws*, 1994 *Commun. Math. Phys.* **159** 195

[18] Boucher C, Ellis R S and Turkington B, *Derivation of maximum entropy principles in two-dimensional turbulence via large deviations*, 2000 *J. Stat. Phys.* **98** 1235

[19] Bouchet F and Corvellec M, *Invariant measures of the 2d Euler and Vlasov equations*, 2010 *J. Stat. Mech.* P08021

[20] Salmon R, *The shape of the main thermocline, revisited*, 2010 *J. Mar. Res.* **68** 541

[21] Dubinkina S and Frank J, *Statistical relevance of vorticity conservation in the Hamiltonian particle-mesh method*, 2010 *J. Comput. Phys.* **229** 2634

[22] Turkington B and Whitaker N, *Statistical equilibrium computations of coherent structures in turbulent shear layers*, 1996 *J. Sci. Comput.* **17** 1414

[23] Whitaker N and Turkington B, *Maximum entropy states for rotating vortex patches*, 1998 *Phys. Fluids* **6** 3963

[24] Robert R and Sommeria J, *Relaxation towards a statistical equilibrium state in two-dimensional perfect fluid dynamics*, 1992 *Phys. Rev. Lett.* **69** 2776

[25] Thess A and Sommeria J, *Intertial organization of two-dimensional turbulent vortex sheet*, 1994 *Phys. Fluids* **6** 2417

[26] Cohen O and Mukamel D, *Ensemble inequivalence: Landau theory and the abc model*, 2012 *J. Stat. Mech.* P12017

[27] Salmon R, 1998 *Lectures on Geophysical Fluid Dynamics* (Oxford: Oxford University Press)

[28] Bouchet F, Morisson P J, Thalabard S and Zaboronksi O, *On Louville's theorem for non-canonical Hamiltonian systems with application to fluid and plasma dynamics. A special class of stationary flows for the two-dimensional Euler equations: a statistical mechanics description*, 2012 Preprint, submitted

[29] Robert R, *On the statistical mechanics of the 2d euler equations*, 2000 *Commun. Math. Phys.* **212** 245

[30] Newman M and Barkema G, 1999 *Monte Carlo Methods in Statistical Physics* (Oxford: Clarendon)

[31] Juttner B and Thess A, *On the symmetry of self-organized structures in two-dimensional turbulence*, 1995 *Phys. Fluids* **7** 2108

[32] Onsager L, *Statistical hydrodynamics*, 1949 *Nuovo Cimento Suppl.* **6** 279

[33] Mikelic A and Robert R, *On the equations describing a relaxation toward a statistical equilibrium state in the two-dimensional perfect fluid dynamics*, 1998 *SIAM J. Math. Anal.* **29** 1238

[34] Venaille A and Bouchet F, *Statistical ensemble inequivalence and bicritical point for two-dimensional flows and geophysical flows*, 2009 *Phys. Rev. Lett.* **10** 104501